

In-plane hole density in $(\text{Ca}_{0.1}\text{La}_{0.9})(\text{Ba}_{1.65}\text{La}_{0.35})\text{Cu}_3\text{O}_y$; nuclear resonance study over the full doping range

Amit Kanigel* and Amit Keren
Technion - Israel Institute of Technology.
 (Dated: May 10, 2018)

We report in-plane ^{63}Cu Nuclear Magnetic Resonance measurements for a series of fully enriched $(\text{Ca}_{0.1}\text{La}_{0.9})(\text{Ba}_{1.65}\text{La}_{0.35})\text{Cu}_3\text{O}_y$ powder samples, which belong to the YBCO family, but the doping could vary from very underdoped to extremely overdoped. From these measurements we determine the average nuclear quadrupole resonance frequency ν_Q , and its second moment $\Delta\nu_Q$, both set by the in-plane hole density n , as a function of oxygen level y . We find that in the overdoped side n is saturated, but $\Delta\nu_Q$ rapidly increases with increasing y . The relevance of these results to the increasing penetration depth in overdoped cuprates is discussed.

A common feature in the phase diagram of all cuprate high temperature superconductors (HTSC) is the dome-shaped curve of the T_c versus doping, divided by an optimal doping point, and different properties on each side. For example: the underdoped samples have a linear temperature-dependent resistivity, while the overdoped samples seem to act like normal metals with T^2 -dependent resistivity. A pseudo-gap is found in the underdoped side, but is absent from the overdoped side. The magnetic penetration depth λ has a minimum at optimal doping^{1,2,3,4}. In contrast Hall measurements⁵ done in single crystals of $\text{La}_{2-x}\text{Sr}_x\text{CuO}_4$ (La214), for example, show a smooth increase in the hole density with increasing doping. This peculiar behavior led to the general belief that the underdoped and overdoped regimes should be treated by different theories. While the overdoped side is believed to adhere to mean field theory similar to the BCS, the presence of strong electronic correlation in the underdoped side motivated the development of exotic theories for this regime. Yet, few authors found in the past that contrary to common belief, the hole density is saturated in the overdoped side; for example in La214⁶, $\text{Bi}_2\text{Sr}_2\text{CaCu}_2\text{O}_{8+\delta}$ (Bi2212) and $\text{Tl}_2\text{Ba}_2\text{CuO}_{6+\delta}$ (Tl2201)⁷, and $\text{HaBa}_2\text{CuO}_{4+\delta}$ (Ha124)⁸. This possibility could change the way we think about overdoped cuprates. However, up until now, it could not be tested for the very popular and most homogenous $\text{YBa}_2\text{Cu}_3\text{O}_y$ (Y123) system since it could not be overdoped without introducing disorder, e.g., by doping with Ca.

In this letter we overcome this problem by investigating the fully enriched cuprate system $(\text{Ca}_{0.1}\text{La}_{0.9})(\text{Ba}_{1.65}\text{La}_{0.35})\text{Cu}_3\text{O}_y$ (CLBLCO). This system is unique in the sense that doping can vary across the full range, from the very underdoped to the extreme overdoped, without any structural changes⁹. The system belongs to the Y123 family, but it is tetragonal over the entire doping range, with no preferred direction for the CuO chains and no chain ordering. Doping is controlled only by the oxygen level⁹. We determine the doping level by extracting the nuclear quadrupole resonance parameter ν_Q from ^{63}Cu Nuclear Magnetic Resonance (NMR) measurements. The Cu, with its spin 3/2 nuclei, is directly coupled to charge degrees of freedom via the

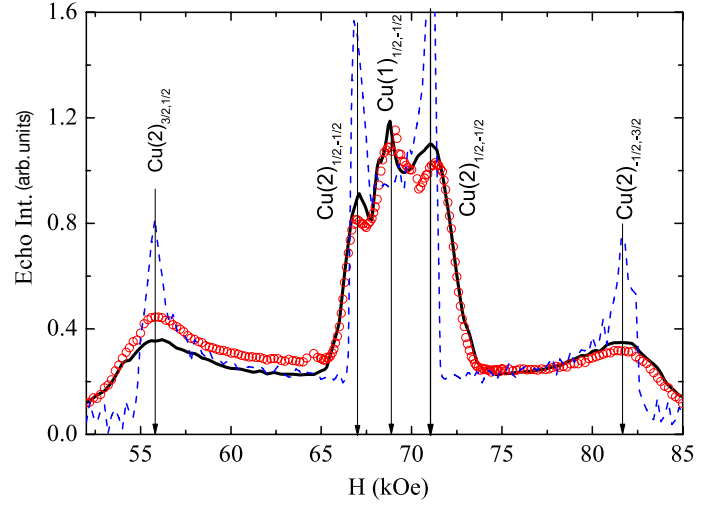


FIG. 1: (Color online) Symbols: The spectra of the optimally doped CLBLCO sample ($y = 7.135$). Dashed line: Powder line shape reconstructed using the parameters found by solving Eqs. 4. Solid line: Best fit to the data by taking into account a distribution of ν_Q .

electric field gradient (EFG), and ν_Q is a measure of this coupling. ν_Q , in turn, depends linearly on the hole density¹¹ n according to

$$\nu_Q = An + \nu_Q^0 \quad (1)$$

where A and ν_Q^0 are doping-independent. This linear dependence was demonstrated for various compounds such as Y123¹², La214¹³, and Ha124¹⁴. Therefore, Eq. 1 and the ability of NMR to detect the in-plane cooper $[\text{Cu}(2)]$ ν_Q selectively, will allow us to determine the carrier concentration in the overdoped regime.

The measurements were done on powder samples since CLBLCO is not orientable. Their preparation is described in Ref.⁹. The oxygen content was measured by double Iodometric titration. The accuracy of this method in enriched CLBLCO is about 0.01. We measured seven different samples in the normal state at 100 K. The most overdoped sample is not superconducting. The NMR

measurements were done by sweeping the field in a constant applied frequency $f_{\text{app}} = 77.95$ MHz using a $\pi/2 - \pi$ echo sequence. The echo signal was averaged 100,000 times and its area evaluated as a function of field. The full spectrum of the optimally doped sample ($y = 7.135$) is shown in Fig. 1. Four peaks associated with the plane Cu(2) and one peak from the Cu(1) can be clearly seen.

A zoom on the main features of the Cu(2) signal of all seven samples is depicted in Fig. 2 (note the three axis breakers). The evolution of the main peaks with doping from underdoped to the optimally doped ($y = 7.135$) samples is highlighted by the dotted line. This line is extended to the overdoped samples to demonstrate their opposite peak position evolution with doping. For overdoped samples, arrows indicate the peak positions. The opposite peak position evolution of the overdoped samples is the main analysis independent finding of this work. It shows that charge density in the CuO_2 plane is not increasing in the overdoped side.

The Cu spin Hamiltonian can be written as¹⁵:

$$\mathcal{H}/h = -\nu_l \mathbf{I} \cdot (\mathbf{1} + \mathbf{K}) \cdot \hat{\mathbf{H}} + \frac{\nu_Q}{6} [3\mathbf{I}_z^2 - \mathbf{I}^2 + \eta(\mathbf{I}_x^2 - \mathbf{I}_y^2)] \quad (2)$$

where $\nu_l = (63\gamma/2\pi)H$, $\hat{\mathbf{H}}$ is a unit vector in the direction of the field, \mathbf{K} is the shift tensor, and η is the asymmetry parameter of the EFG. In the absence of magnetic field, there is only one transition frequency given by $f = \nu_Q \sqrt{1 + \eta/3}$, so ν_Q cannot be separated from η , and the use of the magnetic field is essential. This field, applied in the direction θ and ϕ with respect to the principal axis of the EFG, lifts this degeneracy and three transition frequencies $\nu_m(H, \theta, \phi)$ are expected: a center line which correspond to the $1/2 \rightarrow -1/2$ transition ($m = 0$), and two satellites which corresponds to the $3/2 \rightarrow 1/2$ ($m = 1$) and $-1/2 \rightarrow -3/2$ ($m = -1$) transitions. Expressions for $\nu_m(H, \theta, \phi)$ up to second order perturbation theory in ν_Q for completely asymmetric EFG and shift tensors are given in Ref.¹⁶.

For calculating a field-swept powder spectrum $P(H)$ one has to evaluate

$$P_m(H) \propto \sum_m \int M^2 \delta[f_{\text{app}} - \nu_m(H, \theta, \phi)] d\Omega \quad (3)$$

where M is a matrix element. This spectrum is known to have four peaks (two emerge from $m = 0$) at fields given^{16,17} by

$$f_{\text{app}} = \frac{1}{2}\nu_Q(1 - \eta) + \nu_{ls} \quad (4a)$$

$$f_{\text{app}} = \frac{\nu_Q^2}{48\nu_{lc}}(9 - 6\eta + \eta^2) + \nu_{lc} \quad (4b)$$

$$f_{\text{app}} = -\frac{\nu_Q^2}{3\nu_{hc}}(1 - \eta) - \frac{4(K_{\perp} - K_z)^2\nu_{hc}^3}{3\nu_Q^2(\eta - 3)^2} - \frac{2K_{\perp}(\eta - 2) + K_z(\eta - 5) + 3(\eta - 3)}{3(3 - \eta)}\nu_{hc} \quad (4c)$$

$$f_{\text{app}} = -\frac{1}{2}\nu_Q(1 - \eta) + \nu_{hs} \quad (4d)$$

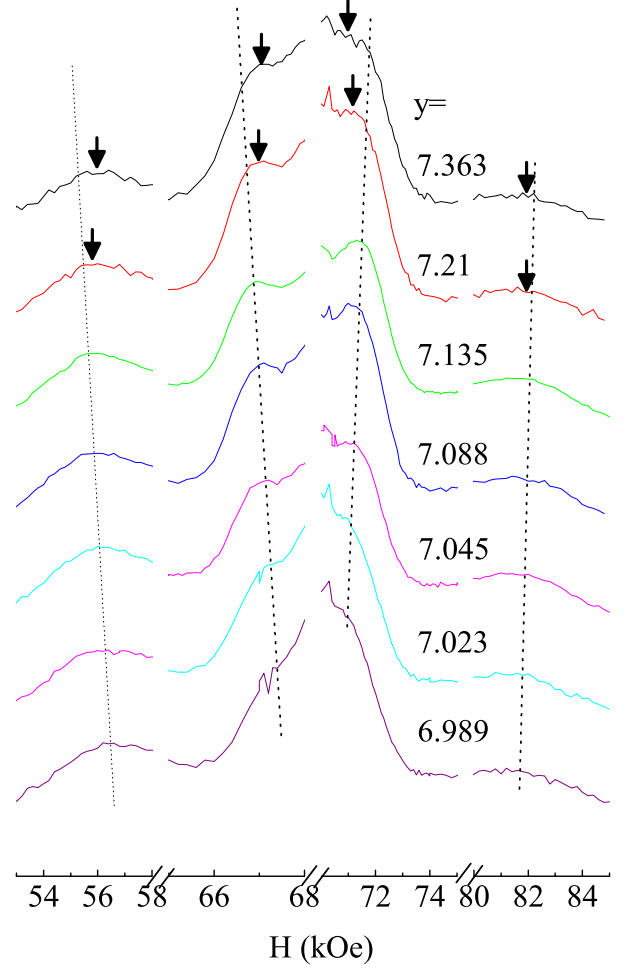


FIG. 2: (Color online) Spectra for the 7 CLBLCO samples. Position of the four peaks associated with the plane Cu as function of doping from under to optimal ($y = 7.135$) doping are shown by the dotted lines. These lines are extended further to show the opposite peak position evolution for overdoped samples. Their peak position are shown by arrows.

where ν_{ls} , ν_{lc} , ν_{hc} , ν_{hs} are the low satellite, low center, high center, and high satellite peaks, respectively, and we assume $K_x = K_y = K_{\perp}$ since CLBLCO is tetragonal. Usually one can extract all the averaged Hamiltonian parameters from the position of the peaks in the spectra by solving Eqs. 4 numerically¹⁷. However, we are interested in both the parameters and their distribution. Therefore, we use a grid in the (θ, ϕ) space, calculate the frequency $\nu_m(H, \theta, \phi)$ for every m , field, and point on the grid, and add 1 to a histogram of H when this frequency equals f_{app} . The matrix elements are taken as unity. The nu-

merical summation approximates $P(H)$ in Eq. 3.

This numerical approach is demonstrated in Fig. 1 where the four peaks associated with Cu(2) have almost axial symmetry ($\eta \sim 0$), and the fifth (middle) peak is from Cu(1) which has a completely asymmetric EFG ($\eta \sim 1$). The dashed line in Fig. 1 is the powder line shape calculated after the parameters for Cu(2) were extracted by solving Eqs. 4 for the plane site. The singularities of the theoretical line agree with the peaks in the NMR data, as expected. However, the overall shape of the calculated line does not resemble the data at all, the reason being the distribution of the Hamiltonian parameters. The main contribution to the width, of the order of a few MHz, is from a distribution in ν_Q , since the quadrupole interaction is the only interaction of such magnitude in the system. To account for this distribution we simulated the line shape by adding to the numerical evaluation of Eq. 3 a loop over 200 values of ν_Q drawn from a normal distribution with a width $\Delta\nu_Q$. We also added the contribution of the chain site, with $\eta \sim 1$ and removed the $K_x = K_y = K_\perp$ constrain, to take into account possible local orthorhombic distortions. We searched for the best fit to the data by χ^2 minimization using a simplex code¹⁸. The result for the optimally doped sample is shown as the solid line in Fig. 1.

In Fig. 3 we show the position of the four peaks (shown in Fig. 2) as a function of doping. The separation between the satellites increases with doping up to the optimal doping point and decreases as the system is overdoped. The evolution of the width of the center lines can be seen by examining the peaks of the center lines in Fig. 2.

By solving Eqs. 4, we calculate ν_Q , η , K_z and K_\perp for all the samples. The calculated ν_Q s are shown in Fig. 4. All parameters are used as the initial guess in the fitting program. The results for fitted ν_Q and $\Delta\nu_Q$ are also shown in Fig. 4. The solid lines in this figure are guides for the eye. The width of the lines does not allow us to determine η , K_z , K_x and K_y very accurately. In general the Cu(2) η is always very small for all the samples, ranging from 0.015 for the optimal doped sample and up to 0.07 for the underdoped sample, in agreement with Y123¹⁹. We have also attempted to fit the data starting from arbitrary initial guess. This gave somewhat different fit values. The error bars in Fig. 4 are estimated from the different fit procedures. These error bars are larger by a factor of 4 than the error bars calculated by the fitting program itself.

The location of the simulated peaks agrees with the data for all samples, but the simulation program yields a higher ν_Q than extracted from Eqs. 4. The reason is that the theoretical peaks for zero $\Delta\nu_Q$ are not symmetric (see dashed line in Fig. 1). By introducing a normal distribution of ν_Q the peaks tend to shift towards the center of the line resulting in what seems to be a smaller average ν_Q . The computer fit program corrects for this effect by selecting a higher average ν_Q than the initial guess (based on Eqs. 4). We believe that the fit results represent the data better than the calculation that is based on

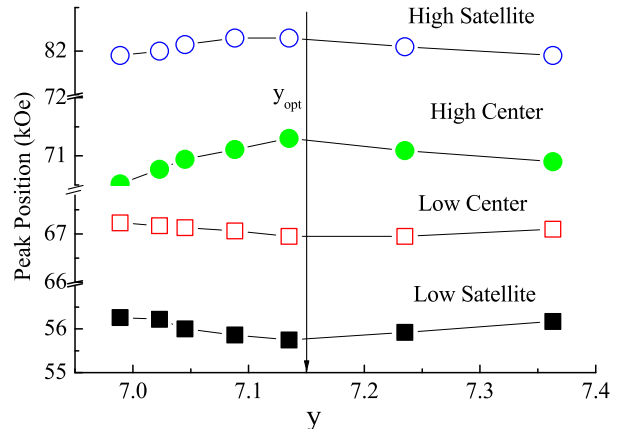


FIG. 3: (Color online) Position of the 4 peaks associated with the plane Cu as function of doping.

the peaks alone.

The results indicate that ν_Q grows linearly with doping in the underdoped side of the phase diagram in agreement with other compounds^{12,13,14}. In the overdoped side ν_Q grows very slowly with doping and saturates; it does not decrease as one might think looking at the peaks position only. This is due to the increase in $\Delta\nu_Q$. The width decreases with doping, having a minimum at optimal doping, and increases quite sharply in the overdoped side. We emphasize, that the main result, a deviation from the linear dependence of ν_Q in the overdoped side, is observable in the raw data itself. The same result is supported both by the exact solution of Eqs. 4 and by the numerical fits.

The fact that there is a sudden change in the ν_Q versus y relation suggests a change in the doping mechanism itself. In CLBLCO, like in Y123, the doping is done by adding oxygen ions into the plane of chains, which are initially only half full. Our result suggests that in the underdoped region a constant part of the introduced holes goes into the CuO_2 plane. After crossing the optimal doping point, most of the holes remain in the chains.

Recent density functional calculations of doping and its effect on the EFG²⁰ in YBCO show that both ν_Q and the doping should go through a maximum as a function of the oxygen level. It should be noted that resistivity and Hall measurements in YBCO will be less sensitive to the change in the plane doping mechanism since above optimal doping the chain layers start to conduct.

Thus, above optimal doping the energetic cost of adding a free hole to the CuO_2 plane increases. Trying to overdope CLBLCO results in transfer of charge into the chains. Moreover, attempts to overdope the sample, leads to higher degree of disorder in the plane, manifested in the increase of $\Delta\nu_Q$. This is the main conclusion of this work.

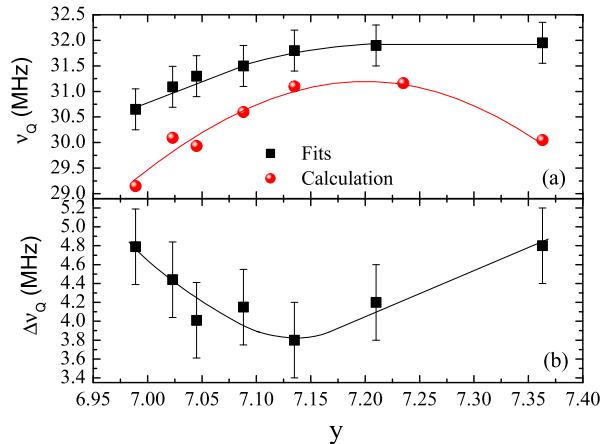


FIG. 4: (Color online) (a) ν_Q , the mean value of the quadrupole frequency, versus doping as obtained by fit and calculation described in the text. (b) $\Delta\nu_Q$, the width of the normal distribution around ν_Q obtained by the fit.

Finally, it is interesting to compare the NQR results with previous magnetic penetration depth, λ , measurements⁴. λ was determined by transverse field muon spin rotation where the relaxation rate σ is proportional to λ^{-2} [ref²¹]. In CLBLCO σ is proportional

to T_c in both the under and over doped sides, with the same proportionality constant of all HTSC, obeying the Uemura relation⁴. Within the clean limit BCS theory framework, at $T = 0$ all the normal state carriers should pair and condensate giving $\sigma \propto n_s/m^*$ where $n_s = n/2$ and the effective mass is just twice the effective mass of the quasi-particle in the normal state. Therefore, the saturation of the number of holes in the plane above optimal doping cannot explain the reduction in σ alone. Clearly the explanation must involve a combination of the saturation of the normal state carrier density and some other mechanism. Few suggestion for the nature of this mechanism were proposed, for example, phase separation and creation of metallic droplets¹, and pair breaking². The fact that we find an increase in the width of the charge distribution in the planes might be an important ingredient in the correct theory explaining the peculiar behavior of the superfluid density in the overdoped side.

In summary, we have managed to measure the average quadrupole resonance parameter ν_Q and the width of its distribution $\Delta\nu_Q$, for the in-plane Cu, in a system belonging to the YBCO family but where doping can vary from heavily underdoped to extreme overdoped. We find that ν_Q increases with oxygen doping in the underdoped side but is saturated in the overdoped side. In contrast, $\Delta\nu_Q$ has a minimum at optimal doping.

We acknowledge useful discussion with Y. Eckstein and the help of Arkady Knizhnik with the Iodometric titration. This work was funded by the Israeli Science Foundation.

* Current Address: Department of Physics, University of Illinois at Chicago, IL 60607

¹ Y.J. Uemura, A. Keren, L.P. Le, G.M. Luke, W.D. Wu, Y. Kubo, T.Manako, Y. Shimakawa, M. Subramanian, J. L. Cobb and J. T. Markert Nature, **364** 605 (1993).

² Ch. Niedermayer, C. Bernhard, U. Binniger, and H. Glckler Phys. Rev. Lett., **71** 1764 (1993).

³ J.P. Locquet, Y. Jaccard, A. Cretton, E. J. Williams, F. Arrouy, E. Mchler, T. Schneider, O. Fischer and P. Marti-noli Phys. Rev B, **54**, 7481 (1996).

⁴ A. Keren, A. Kanigel, J. S. Lord and A. Amato Solid State Comm., **126** 39 (2003).

⁵ Yoichi Ando, A. N. Lavrov, Seiki Komiya, Kouji Segawa, and X. F. Sun Phys. Rev. Lett., **87**, 017001 (2001).

⁶ S. Uchida, T. Ido, H. Takagi, T. Arima, Y. Tokura, and S. Tajima Phys. Rev. B, **43** 7942 (1991).

⁷ A. V. Puchkov, P. Fournier, T. Timusk, and N. N. Kolesnikov Phys. Rev. Lett, **77**, 1853 (1996).

⁸ R. Puzniak, R. Usami and H. Yamauchi Phys. Rev. B **53**, 86 (1996).

⁹ D. Goldschmidt, A. Knizhnik, Y. Direktovitch, G. M. Reiser, and Y. Eckstein Phys Rev. B **49**, 15928 (1994).

¹⁰ Y.J. Uemura Solid State Comm. **120** , 347 (2001).

¹¹ Kunisuke Asayama, Yoshio Kitaoka, Zheng Guo-qing and Kenji Ishida Prog. Nuc. Mag. Reso. Spec., **28**, 221 (1996).

¹² H.Yasuoka, in Spectroscopy of Mott Insulator and Corre-

lated Metals, edited by A. Fujimori and Y. Tokura, Solid State Sciences, Vol. 119 (Springer-Verlag, Berlin, 1995), p. 213.

¹³ Guo-qing Zheng, Yoshio Kitaoka, Kenji Ishida and Kunisuke Asayama, J. Phys. Soc. Jpn. **64**, 2524 (1995).

¹⁴ A. A. Gippius, E.V. Antipov, W. Hoffmann and K. Luders, Physica C **276**, 57 (1997).

¹⁵ C.P. Slichter Principles of Magnetic Resonance, Harper and Row, New York, (1963).

¹⁶ J. F. Baugher, P.C. Taylor, T. Oja and P.J. Bray J. of Chem. Phys., **50**, 4914 (1969).

¹⁷ A. Keren, P. Mendels, M. Horvati?, F. Ferrer, Y. J. Uemura, M. Mekata and T. Asano Phys. Rev. B **57**, 10745 (1998).

¹⁸ W.H. Press, B.P. Flannery, S. Teukolsky and W.T. Vetterling, numerical Recipes in C, Cambridge University Press (1988).

¹⁹ C. H. Pennington, D. J. Durand, D. B. Zax, C. P. Slichter, J. P. Rice, and D. M. Ginsberg, Phys. Rev. B **37**, R7944 (1988); T. Shimizu *et al.*, Journal of the Physical Society of Japan, **57**, 2494 (1988).

²⁰ E. P. Stoll and P. F. Meier, Private Communication.

²¹ Muon Science: Muons in Physics, Chemistry and Materials, Eds S. L. Lee, S. H. Kilcoyne and R. Cywinski (Institute of Physics, London), 1999.